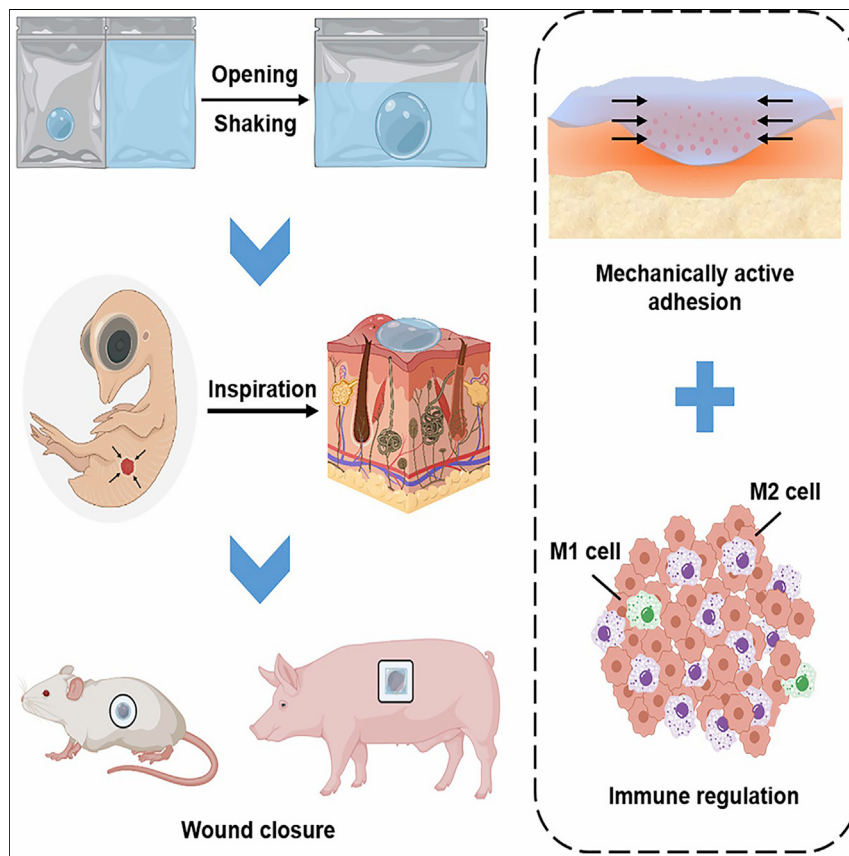


Article

Mechanically active adhesive and immune regulative dressings for wound closure



An easy-to-prepare and ready-to-use hydrogel dressing, inspired by the shrinkage of chicken embryo wounds, was designed for wound closure. Using this wound dressing, a successful wound healing process was achieved in both mouse and porcine wounds, due to mechanically active adhesion and immune regulation.

Jiaying Hu, Ting Wei, He Zhao, ..., Han Zhang, Zhuang Liu, Qian Chen

chenqian@suda.edu.cn

Highlights

Strongly adhesive hydrogel to tissues via covalent cross-linking

Active wound contraction triggered by temperature-sensitive PNIPAm

Modulated inflammatory responses in wound achieved by PMAA

Easy-to-prepare and easily stored wound-healing hydrogel

Demonstrate

Proof-of-concept of performance with intended application/response

4

Hu et al., Matter 4, 2985–3000
September 1, 2021 © 2021 Published by Elsevier Inc.
<https://doi.org/10.1016/j.matt.2021.06.044>



Article

Mechanically active adhesive and immune regulative dressings for wound closure

Jiaying Hu,^{1,3} Ting Wei,^{1,3} He Zhao,² Muchao Chen,¹ Yanjun Tan,¹ Zhaoxin Ji,¹ Qiutong Jin,¹ Jingjing Shen,¹ Yikai Han,¹ Nailin Yang,¹ Linfu Chen,¹ Zhisheng Xiao,¹ Han Zhang,¹ Zhuang Liu,¹ and Qian Chen^{1,4,*}

SUMMARY

Adhesive hydrogels have attracted wide attention as wound dressings. However, conventional wound dressings that passively promote healing usually show limited efficacy. Although various drugs or cells are introduced to drive the healing process, such strategies are limited by the complicated fabrication process. Here, a mechanically active adhesive and immune regulative dressing is developed, mainly consisting of temperature-sensitive hydrogel with semi-interpenetrating network structure. This hydrogel could strongly adhere to and actively contract the wound in a ready-to-use form, where the freeze-dried hydrogel and sterile saline are sealed in two separated packages. More interestingly, the interspersed poly(methacrylic acid) could further promote wound healing via increasing the formation of new blood vessels and modulating inflammatory responses. *In vivo* mouse and porcine wound models validate the accelerated wound healing enabled by active contraction and modulated inflammatory responses. This mechanobiological and immune regulative dressing may provide a new avenue for wound management.

INTRODUCTION

Various types of wounds, including acute postsurgical wounds, traumatic injuries, burns, and chronic wounds resulting from diabetes or circulatory disturbances, remain a central concern in clinic and exert a great impact on patients and society.^{1,2} Wound healing is an important physiological process involving an evolutionarily conserved sequence of hemostasis, inflammation, proliferation, and tissue remodeling. A crucial process during the wound healing response is restoring the epithelial layer to regain the integrity of the skin barrier.^{3–6} Although various wound dressings, such as gauzes, cotton wools, and hydrogels, have been extensively used, existing adhesive wound dressings are not satisfactory in treating large or chronic wounds due to their slow and passive healing behaviors.^{7–11} To promote wound healing, efforts have been devoted to delivering antimicrobial agents to protect wounds from pathogenic infections and bioactive agents such as growth factors or cells to accelerate the cell proliferation and tissue remodeling.¹² Notwithstanding, such functional wound dressings are usually limited by complicated preparation processes, potential side effects associated with drugs, high cost, difficulty in handling and storage, and problems with efficient loading and controlled release of encapsulated bioactive agents.^{13–17}

In addition to encapsulating wound dressings with antimicrobial and bioactive agents to promote wound healing, wide attention has been attracted to regulating

Progress and potential

Conventional wound dressing by passively promoting wound healing usually exhibits unsatisfactory results in treating large or chronic wounds. Inspired by the contraction ability of embryonic wounds, we designed a new kind of mechanically active and immune regulative hydrogel dressing by integrating gelatin and PMAA chains into the main network of temperature-sensitive PNIPAm. Such hydrogel could effectively promote wound healing via strongly adhering to tissues, mechanically contracting the wounds, promoting angiogenesis, depositing collagen, and reducing inflammation. Moreover, such hydrogel exhibits unique ease of preparation and ease of storage properties, which may provide new opportunities for wound healing and has great potential for clinical translation.



the innate immune cells, especially macrophages, which play a key role in promoting tissue regeneration to promote the tissue remodeling.¹⁸ It has been reported that materials based on methacrylic acid (MAA) are able to polarize macrophages toward the pro-regenerative (M2) phenotype.^{19–22} Such polarization of macrophages could further regulate the secretion of inflammation-related cytokines such as interleukin 1 β (IL-1 β), interleukin 10 (IL-10), interleukin 6 (IL-6), and tumor necrosis factor alpha (TNF- α) to promote tissue regeneration. Furthermore, MAA could accelerate wound healing^{23,24} via promoting the neovascularization of surrounding tissues^{20,25} and regulating angiogenesis-associated factors, including platelet-derived growth factor B (PDGF-B), basic fibroblast growth factor (bFGF), thrombospondin 1 (TSP-1), vascular endothelial growth factor (VEGF), and C-X-C motif chemokine10 (CXCL10). Thus, engineering wound dressings with immune regulation ability may be an interesting strategy to promote wound healing without additional drugs.

While current strategies focus on designing wound dressings with biochemical functions, much less attention has been paid to engineering dressings to actively contract the wound with mechanical cues.^{26,27} Inspired by the embryonic wound healing, which exhibits excellent regeneration of fetal skin by forming actin cables to contract and draw wound edges together like purse strings,^{28–30} we design a new kind of wound dressing that can actively adhere to and contract the wound, and effectively modulate inflammatory responses to promote wound healing. Specifically, such a mechanically active and immune regulative PNIPAm-PMAA (PNIPAm-P) hydrogel is synthesized by free radical polymerization of temperature-sensitive monomer N-isopropylacrylamide (NIPAm) forming poly(N-isopropylacrylamide) (PNIPAm) as the main network, and additional poly(methacrylic acid) (PMAA) was introduced to form the semi-interpenetrating network. The unique wound dressing developed in this work was demonstrated to be (1) strongly adhesive to tissues via covalent cross-linking between activated carboxylic groups on the hydrogel and amine groups on the tissue surface, (2) capable of contracting the wounds mechanically due to the thermoresponsive shrinkage ability of PNIPAm, and (3) effective to modulate the inflammatory process and promote neovascularization. Using this wound dressing, a successful wound healing process was achieved in both mouse and porcine wound models. Such new mechanobiological, immune regulative, and drug-free dressings may be useful to accelerate wound healing in different settings.

RESULTS AND DISCUSSION

Preparation and characterization of PNIPAm-P hydrogel

The PNIPAm-P hydrogel was obtained by adding PMAA-Na and gelatin to a chemically cross-linked PNIPAm hydrogel, which was prepared via the traditional free radical polymerization (Figure 1A). In this hydrogel, the main PNIPAm network with temperature-sensitive property was able to mechanically contract the wounds. Moreover, PMAA chains penetrated the hydrogel and formed a semi-interpenetrating network, which endowed the hydrogel with additional immunomodulatory functions, including modulating the polarization of macrophages, controlling the secretion of inflammation-related cytokines, and promoting neovascularization of surrounding tissue, to accelerate the wound healing process.²¹ As a natural macromolecule, gelatin containing hydroxyl groups and carboxylic groups, introduced in the hydrogel network, provides selective and strong binding ability to certain substances. For comparison, non-temperature-sensitive hydrogel (PAAm-PMAA [PAAm-P] hydrogel) and temperature-sensitive hydrogel without PMAA (PNIPAm hydrogel) were also synthesized using a similar method. The chemical components and Fourier transform infrared spectroscopy (FTIR) spectra of three different

¹Institute of Functional Nano & Soft Materials (FUNSOM), Jiangsu Key Laboratory for Carbon-Based Functional Materials & Devices, Soochow University, Suzhou, Jiangsu 215123, China

²Children's Hospital of Soochow University, Pediatric Research Institute of Soochow University, Suzhou, Jiangsu 215123, China

³These authors contributed equally

⁴Lead contact

*Correspondence: chenqian@suda.edu.cn
<https://doi.org/10.1016/j.matt.2021.06.044>

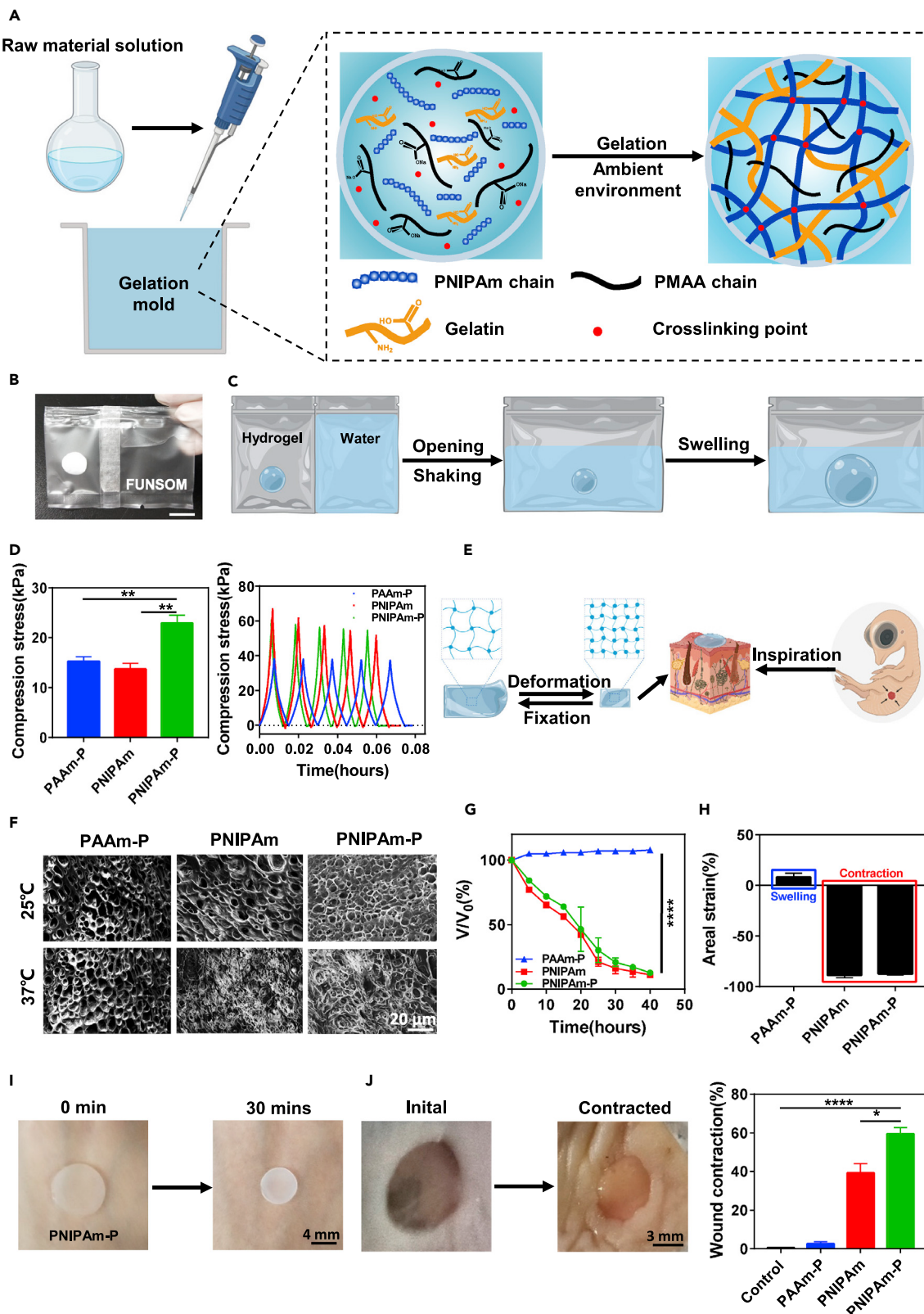


Figure 1. Schematic illustration and characterization of PNIPAm-P hydrogel dressing

- (A) PNIPAm-P hydrogel was formed by mixing NIPAm, PMAA-Na, and gelatin through free radical polymerization.
- (B) Photograph of the hydrogel dressing. The scale bar represents 8 mm.
- (C) Schematic showing the using process of this hydrogel dressing.
- (D) The mechanical properties of various hydrogel matrices, including the hybrid network PAAm-PMAA hydrogel (PAAm-P), the single network PNIPAm hydrogel (PNIPAm), and the hybrid network PNIPAm-PMAA hydrogel (PNIPAm-P).
- (E) Scheme indicating the hydrogel could contract the wounds mechanically due to its temperature-sensitive shrinkage property, inspired by skin wounds of chicken embryo.
- (F) Representative scanning electron microscope image of various hydrogel matrices at different temperatures.
- (G) Curves of volume changes of various hydrogel matrices under equilibrium conditions at 37°C.
- (H) The relationship between areal strain and matrix composition measured under equilibrium conditions at 37°C.
- (I) The active shrinkage behavior of PNIPAm-P hydrogel placed on the hand for 30 min.
- (J) Ex vivo wound contraction of fresh rodent skin using various hydrogel matrices. The representative figures show a wound treated with PNIPAm-P hydrogel.
- All data are presented as mean \pm SEM ($n = 4$). Statistical significance was calculated by one-way ANOVA with a Tukey post hoc test. * $p < 0.05$, ** $p < 0.01$, *** $p < 0.001$, and **** $p < 0.0001$.

hydrogels are shown in [Table S1](#) and [Figure S1](#), respectively. Moreover, considering the abundant carboxylic groups on the surface of hydrogel, 1-(3-dimethylamino-propyl)-3-ethylcarbodiimide hydrochloride (EDC) and N-hydroxy succinimide (NHS) were used to activate carboxylic groups to facilitate the formation of amide bonds between tissues and hydrogels. Thus, the lap-shear test was used to evaluate the adhesive ability of PNIPAm-P hydrogel to skin. As shown in [Figure S2](#), the adhesive energy of PNIPAm-P was significantly higher than that of clinical dressings and bandages, such as Band-Aids ($\sim 8 \text{ J m}^{-2}$). Compared with PNIPAm hydrogel, the addition of PMAA enabled the hydrogel to obtain higher adhesive energy ($\sim 120 \text{ J m}^{-2}$). The appropriate adhesive strength made PNIPAm-P hydrogel a suitable wound sealant. More interestingly, PNIPAm-P hydrogel can be packaged in the commercially available form with freeze-dried hydrogel in the left and sterile saline solution containing EDC and NHS in the right ([Figure 1B](#)). Before use, it is necessary merely to disassemble the middle seal, mix the left and right parts together by shaking, and wait a few minutes for the hydrogel to absorb water and swell ([Figure 1C](#) and [Video S1](#)).

The formation of PNIPAm-P hydrogel was further confirmed by the rheological behavior test. The value of storage modulus (G') was much higher than that of loss modulus (G''), indicating the representative elastic network in PNIPAm-P hydrogel ([Figure S3](#)). To investigate the biocompatibility of the hydrogel, fibroblasts, a kind of cell usually responsible for wound repair,³¹ were cultured in a culture medium containing PNIPAm-P, PNIPAm, or PAAm-P hydrogels. Both the fluorescence optical microscope imaging and 3-[4,5-dimethylthiazol-2-yl]-2,5-diphenyltetrazolium bromide (MTT) assay indicated that all these hydrogels had a negligible effect on the proliferation of fibroblasts ([Figure S4](#)). The loading-unloading compression stress-strain curve further indicated that PNIPAm-P hydrogel could withstand high pressure to complete the deformation without cracking. After removing the compressive loading, the PNIPAm-P hydrogel could automatically and quickly return to its original shape, indicating that the hydrogel showed the desired recyclability ([Figure 1D](#)). The high compressibility and good resilience of PNIPAm-P hydrogel may contribute to the integration of gelatin in the PNIPAm network, together with the non-covalent interactions between PNIPAm, PMAA, and gelatin, which dissipated energy under large deformation and improved the mechanical property of hydrogel.

Thermoresponsive behavior

Embryonic wound healing, which is a kind of perfect regeneration process, involves the formation of actin cables on the front edge of cells and pulling the edges of the

wound together in a purse-like manner.²⁸ Inspired by this unique wound healing process, we leveraged the shrinkage properties of PNIPAm-based hydrogels in the environment with temperature higher than 32°C to prepare the temperature-sensitive shrinkage dressing,^{32,33} which could pull the edges of the wound together in a purse-like manner as embryonic wound healing process to accelerate the wound healing (Figure 1E). In order to verify our vision, we investigated the temperature-triggered contraction behavior of PNIPAm-P hydrogel. According to previous work,^{34–36} PNIPAm chain in aqueous solution could undergo a phase change from homogeneous modality to heterogeneous modality when the temperature was higher than 32°C. Thus, we first studied the changes of space structure in the chemically cross-linked PNIPAm hydrogel by scanning electron microscope imaging. As shown in the scanning electron microscope images, compared with the hydrogel at 25°C, the pore sizes of the temperature-sensitive hydrogels PNIPAm and PNIPAm-P were significantly reduced at 37°C, which indicated that hydrogels containing PNIPAm exhibited excellent temperature-sensitive shrinkage property (Figure 1F).

Moreover, the temperature-triggered contraction behavior of hydrogel was further quantitatively characterized. As shown in Figures 1G and 1H, PNIPAm-P hydrogel shrank to ~85% of its initial volume within 40 min, resulting in an area shrinkage strain of 90%, which was comparable with that observed in PNIPAm hydrogel. Such unique temperature-triggered contraction behavior of this hydrogel encouraged us to explore its ability to contract the wound mechanically. First, we applied the PNIPAm-P hydrogel on our hands, and the shrinkage behavior of hydrogel at body temperature could be clearly observed (Figure 1I). Then, the hydrogel was placed on the isolated rodent skin wound, and incubated at 37°C overnight. After that, the isolated skin wound was quickly frozen with liquid nitrogen to maintain the wound size. As shown in Figure 1J, compared with other groups, the area of wound treated with PNIPAm-P hydrogel effectively reduced by ~60%. Thus, the excellent temperature-triggered contraction behavior of PNIPAm-P hydrogel endows its potential application to mechanically promote wound closure.

Wound healing in mouse model

The PNIPAm-P hydrogel developed in this work was mainly composed of a chemically cross-linked PNIPAm network with thermosensitive behavior and interpenetrating PMAA chains with immunomodulatory functions. This hydrogel was expected to actively contract wound macroscopically and effectively regulate the inflammatory responses and promote neovascularization, which was promising for wound healing. We first evaluated the wound closure effect induced by PNIPAm-P hydrogel in mouse model. Healthy BALB/c mice were randomly divided into four groups: (1) control, (2) PAAm-P, (3) PNIPAm, and (4) PNIPAm-P. After perforating the skin on the backs of mice and fixing the edges of the wounds, three hydrogels were applied to cover the wounds (Figure 2A). The size of wounds was measured every 2 days. It was found that PNIPAm-P exhibited a much better wound closure effect as early as day 4 (Figure 2B). Interestingly, the wound treated with PNIPAm-P hydrogel basically reached a state of complete healing (~90%) on day 10, which was much better than that in other groups, including control group (~55% closure), PAAm-P group (~80% closure), and PNIPAm group (~68% closure).

Encouraged by the obvious wound closure effect caused by PNIPAm-P hydrogel, we further investigated the histological evaluation of neonatal wound tissue through hematoxylin and eosin (H&E) staining on day 10 post different treatments. As reflected in Figure 2C, all samples were covered with a complete skin layer, but the proportion

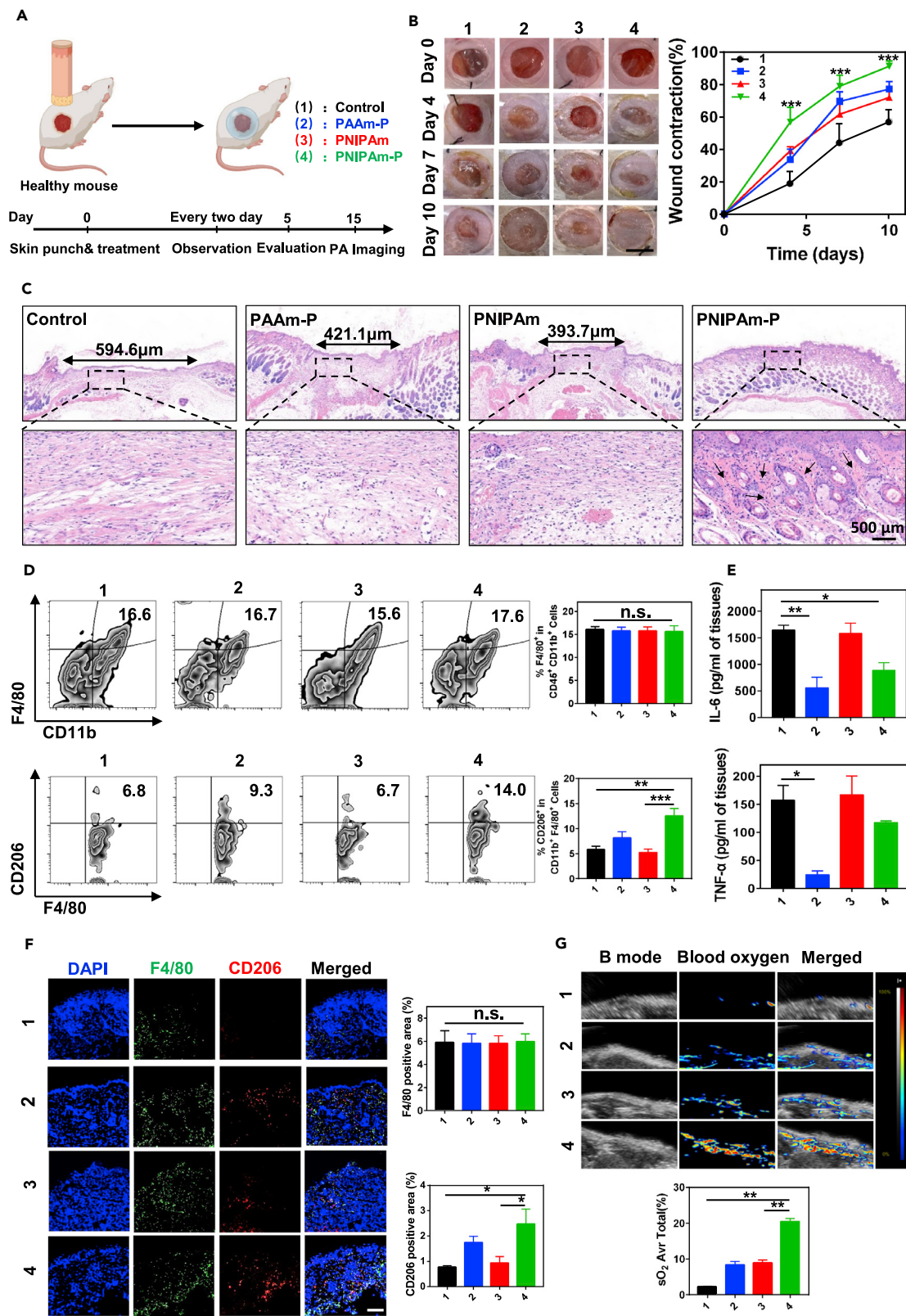


Figure 2. Effects of PNIPAm-P hydrogel on wound healing in mice model

- (A) Schematic illustrating the process of wound healing in BALB/c mice treated with PNIPAm-P hydrogel.
(B) Representative images of the complete wound healing behavior in healthy mice after different treatments. The scale bar represents 5 mm.
(C) H&E staining of histological sections of wound harvested on day 10. The black arrows indicate the ordered collagen fibers.
(D) Representative flow cytometric analysis images and the relative quantification of macrophages ($CD45^+CD11b^+F4/80^+$) and M2-like macrophages ($CD11b^+F4/80^+CD206^+$).
(E) The concentration of inflammation-related cytokines such as IL-6 and TNF- α in wounds on day 5.
(F) Representative immunofluorescence images and the statistical analysis of the expression of F4/80 and CD206 in the wound sections on day 5. The scale bar represents 250 μ m.
(G) Representative photoacoustic images and quantification of the oxyhemoglobin saturation in the newborn wound tissues on day 15.
All data are presented as mean \pm SEM (n = 4). Statistical significance was calculated by one-way ANOVA with a Tukey post hoc test. *p < 0.05, **p < 0.01, ***p < 0.001, and ****p < 0.0001.

of new tissues of the wound treated with PNIPAm-P hydrogel was the smallest, indicating that the wound with PNIPAm-P hydrogel treatment had repaired. Then, the quality of these newly regenerated tissues was further characterized by microscope with higher magnification. As shown in these magnified photomicrographs, ordered collagen fibers and hair follicles were observed in the wound tissue treated with PNIPAm-P hydrogel, further indicating the successful regeneration of wound tissue induced by PNIPAm-P hydrogel. In contrast, there were still extensive granulation tissue in the wound area of the other three control groups. Next, we studied the vascular regeneration in the wound microenvironment post different treatments via immunofluorescent staining using anti-CD31, which is the marker for vascular endothelial cells. As shown in [Figure S6](#), compared with the other three control groups, the expression of CD31 in the wound tissue with PNIPAm-P hydrogel treatment was markedly increased, suggesting that PNIPAm-P hydrogel indeed could promote neovascularization in the wound site. Thus, PNIPAm-P hydrogel could effectively promote wound healing and tissue regeneration.

According to previous literature,^{37–39} in the early stage of tissue repair, activated M1 phenotype macrophages could secrete reactive oxygen species and inflammatory cytokines, and produce high levels of inducible nitric oxide synthase (iNOS), which were responsible for killing microorganisms, removing debris, and promoting inflammation and Th1 responses. In the later part of the repair process, M2 phenotype macrophages could be stimulated by immunomodulatory and anti-inflammatory factors to secrete IL-10, arginase, ornithine, and polyamines, which could further reduce inflammation responses and facilitate cell proliferation and tissue repair. Therefore, M2 phenotype macrophages play an important role in promoting angiogenesis and producing collagen to promote tissue regeneration. Moreover, such polarization of macrophages could further regulate the secretion of inflammation-related cytokines to promote tissue regeneration. Thus, we first investigated the polarization of macrophages around the wound on day 5 post different treatments by flow cytometry. It was discovered that the total number of macrophages in the wounds treated with different hydrogels remained nearly unchanged, while the percentage of M2 phenotype macrophages around the wounds treated with PNIPAm-P hydrogel showed an obvious increase and M1 phenotype macrophages showed a decrease ([Figures 2D, S7, and S9](#)). In addition, immunofluorescence staining was used to assess the expression of F4/80 (a marker for macrophages) and CD206 (a marker for M2 phenotype macrophages) in the wounds. As shown in [Figure 2F](#), compared with the other three groups, the level of F4/80 in the wounds treated with PNIPAm-P hydrogel exhibited little change and the expression of CD206 significantly increased, further verifying that PNIPAm-P hydrogel could effectively promote the polarization of macrophages from pro-inflammatory phenotype (M1 type) to anti-inflammatory phenotype (M2 type).

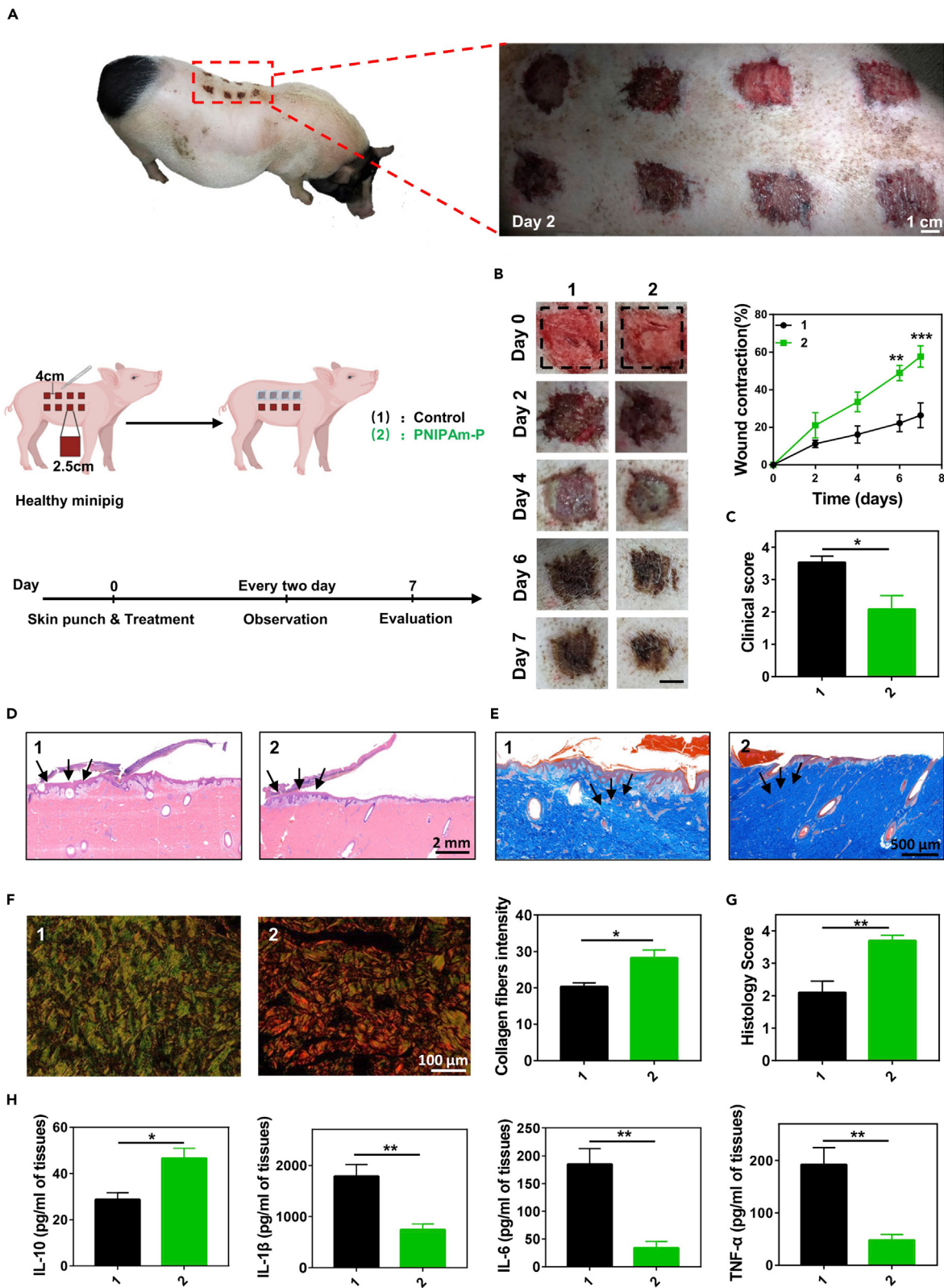


Figure 3. Effects of PNIPAm-P hydrogel on wound healing in porcine wound model

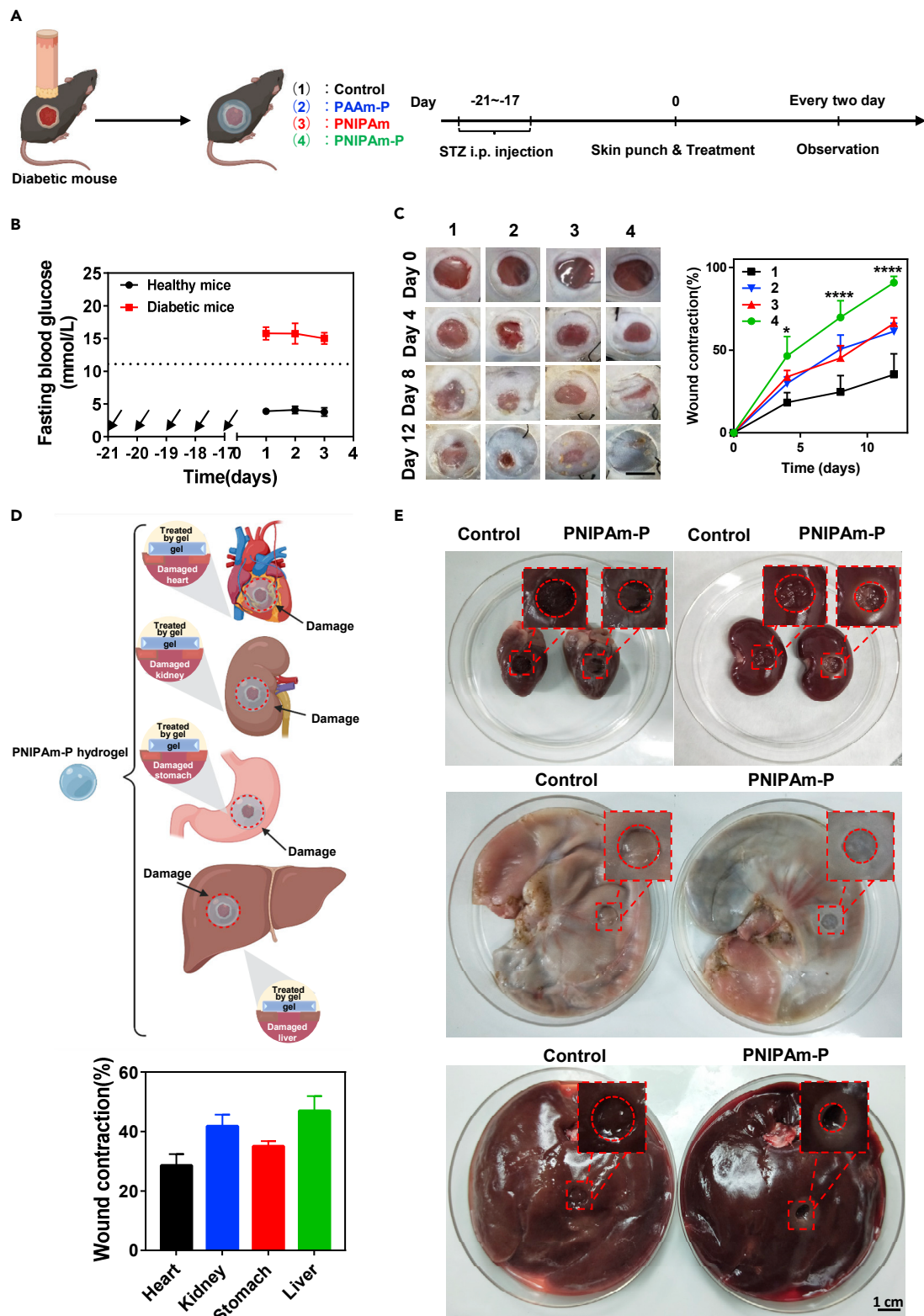
(A) Schematic illustrating the process of wound healing in Bama minipig treated with PNIPAm-P hydrogel.
(B) Representative images of wound on day 0, 2, 4, 6, and 7 post wounding and wound healing behavior after the treatment. The scale bar represents 1 cm.
(C) Clinical scoring of wounds on day 7 by a blinded pathologist expert.
(D) H&E staining of histological sections of wound harvested on day 7. The black arrows indicate the newborn tissues.
(E) Masson trichrome staining of histological sections of wound harvested on day 7. The black arrows indicate the tightness of collagen fibers.
(F) PSR staining of histological sections of wound harvested on day 7.
(G) H&E-stained sections of porcine wound were examined and scored by an experienced veterinary pathologist in a blinded manner.
(H) The concentration of inflammation-related cytokines, including IL-10, IL-1 β , IL-6, and TNF- α , in the wounds on day 7 after treatment.
All data are presented as mean \pm SEM ($n = 4$). Statistical significance was calculated by two-tailed Student's t test. * $p < 0.05$, ** $p < 0.01$, *** $p < 0.001$, and **** $p < 0.0001$.

Then, enzyme linked immunosorbent assay (ELISA) was used to evaluate the expression of inflammation-related cytokines at the wound site. It is worth noting that various pro-inflammatory cytokines, including TNF- α and IL-6, were obviously down-regulated in the wound treated with PNIPAm-P hydrogel, and their concentration was slightly higher than that in the wound treated by PAAm-P hydrogel, which may be due to the smaller pore size of PNIPAm-P hydrogel at body temperature limiting the exposure of PMAA (Figures 2E and S10). Finally, in order to evaluate the formation of functional blood vessels, the blood oxygenation level in the wound lesions after different treatments was detected by ultrasound and photoacoustic imaging on day 15. As shown in Figure 2G, compared with the other three control groups, the wound treated with PNIPAm-P hydrogel showed significantly higher average blood oxygen level. These results indicated that PNIPAm-P hydrogel was able to promote wound healing and angiogenesis through multiple mechanisms, including being strongly adhesive to tissues to protect the wound site from microorganisms, infection, or pollution; contracting the wounds mechanically due to the thermoresponsive shrinkage ability induced by PNIPAm; and changing the polarization of macrophages and promoting angiogenesis by PMAA.

Wound healing in porcine wound model

Encouraged by the effective wound healing process induced by PNIPAm-P hydrogel in the mouse model, we further wanted to explore the application of PNIPAm-P hydrogel in a wound model that is similar to human. Thus, a partial-thickness wound model in Bama minipig was used. In this experiment, a clinical mimicking situation for wound treatment was created. The wounds were treated with or without PNIPAm-P hydrogel and then covered with additional medical bandages. The wounds were observed and recorded every 2 days (Figure 3A). Both the control and PNIPAm-P-treated wounds showed no obvious signs of inflammation and infection. Interestingly, compared with the control wound, the wound treated by PNIPAm-P hydrogel exhibited an accelerated wound healing process and improved clinical score. On day 7, the PNIPAm-P hydrogel-treated wound reached a healing rate close to 60%, while the control wound only achieved a healing rate of 20% (Figures 3B and 3C and Table S2). Then, H&E and Masson trichrome staining were used to further study the wound repair process in the porcine partial-thickness wound model. As shown in Figure 3D, thick granulation tissue was observed in the wound treated with PNIPAm-P hydrogel, while the control wound showed only a thin layer of granulation tissue. Moreover, the collagen deposition behavior after different treatments was observed in the Masson trichrome staining images. As we expected, the wound treated by PNIPAm-P hydrogel showed dense and parallel arrangement of collagen fibers, which could further reduce the formation of scars in the wound area (Figure 3E).

According to previous studies, during the process of damaged skin wound repairing, the ratio of type I and type III collagen is an important parameter to evaluate the

**Figure 4. Other biological applications**

(A) Schematic illustrating the process of wound healing in diabetic mice.

(B) Fasting blood glucose levels of mice after STZ injection to confirm the establishment of diabetic mouse model.

Figure 4. Continued

(C) Representative images of wound on day 0, 2, 4, and 6 post wounding and quantification of wound closure in diabetic mice. The scale bar represents 5 mm.

(D and E) Representative images and quantification of ex vitro tests of PNIPAm-P hydrogel-enabled defect area contraction on fresh rabbit heart, kidney, stomach, and liver.

All data are presented as mean \pm SEM ($n = 4$). Statistical significance was calculated by one-way ANOVA with a Tukey post hoc test. * $p < 0.05$, ** $p < 0.01$, *** $p < 0.001$, and **** $p < 0.0001$.

healing of skin wounds and the formation of scars.⁴⁰ At the early stage of wound repair, type III collagen is the main product, and, after a period of time, type I collagen replaces type III collagen to become the main collagen in the skin.⁴¹ Thus, the slices of skin tissue were collected and stained with the picrosirius red (PSR) on day 5 after the treatment, and then imaged by the polarizing microscope. As shown in Figure 3F, the wound treated with PNIPAm-P hydrogel mainly exhibited type I collagen fiber (yellow or red), and the collagen arrangement was similar to that of normal skin. However, in the control wound, type III collagen fibers (green) occupied the majority. Thus, PNIPAm-P hydrogel could promote the generation of type I collagen fiber and inhibit the formation of scars.

Then, the above H&E, Masson trichrome, and PSR staining sections of Bama minipig wound biopsies were blindly evaluated by an experienced veterinary pathologist (M.P.). The histology scores were evaluated according to the tissue structure, epithelial formation, granulation tissue, inflammatory cells, and abscesses with the 0–5 scoring standard (5 points is the highest score). Five areas from each wound section were recorded by the 10 \times objective, which covered 90%–100% of the wound. The histology score indicated that the wound treated by PNIPAm-P hydrogel showed rapid skin regeneration and fewer visible scars, further demonstrating that PNIPAm-P hydrogel could effectively promote tissue reconstruction and provide non-invasive support for skin integration and repair (Figure 3G). Furthermore, the concentrations of pro-inflammatory cytokines, including IL-6 and TNF- α , were obviously reduced and the concentrations of anti-inflammatory cytokines such as IL-10 showed significant increase (Figure 3H). Taken together, this PNIPAm-P hydrogel could effectively promote wound healing in the porcine partial-thickness wound model, which is closer to the human skin wounds, showing great potential for clinical transformation in the future.

Other tissue repairing applications

Diabetic wounds, one kind of chronic dermal wounds, are difficult to heal due to the diabetic hyperglycemia, lack of oxygen and nutrients, and high level of oxidative stress around the wound.^{42–46} Considering the mechanically contracted activity and immunomodulatory ability of PNIPAm-P hydrogel, we further employed this hydrogel to cure diabetic wounds. First, the diabetic mice model was induced by intra-peritoneal injection of streptozocin (STZ) to healthy C57BL/6 mice according to the standard protocol.^{47,48} As shown in Figure 4B, the fasting blood glucose level of C57BL/6 mice exceeded 11.1 mmol/L for three consecutive days after STZ injection (50 mg/kg per mouse for 5 days), indicating that the diabetic mouse model was successfully established. Then, the diabetic mice were divided into four groups: (1) control, (2) PAAm-P, (3) PNIPAm, and (4) PNIPAm-P (Figure 4A). As we expected, an obvious improvement of wound closure was observed in PNIPAm-P hydrogel-treated group as early as day 4. It was found that the diabetic wounds treated by PNIPAm-P hydrogel were healed to 46% on day 4, which was much higher than other groups (~17% for control, ~30% for PAAm-P, and ~33% for PNIPAm), indicating that the unique PNIPAm-P hydrogel could expedite wound healing in diabetic wounds.

Besides, in order to explore the potential application of PNIPAm-P hydrogel for tissue repair, proof-of-principle applications using *ex vivo* rabbit organ models were carried out. The PNIPAm-P hydrogel was applied to the defect area of different isolated organs, including heart, kidney, stomach, and liver, to investigate its contraction behavior (Figure 4D). As shown in Figure 4E, our PNIPAm-P hydrogel indeed could effectively promote the contraction of the defect area in different organs, especially in the liver, indicating the potential of PNIPAm-P hydrogel with active contraction behavior for *in vivo* tissue repair. Although the above results indicated the possible applications of PNIPAm-P hydrogel in chronic wounds and *in vivo* tissue repair, the long-term efficacy, biodegradability, and biological response caused by PNIPAm-P in the relevant clinical environment still need further research.

Conclusion

In conclusion, a novel mechanically active adhesive and immune regulative PNIPAm-P hydrogel dressing was developed to accelerate wound healing. This PNIPAm-P hydrogel exhibits many unique advantages over existing tissue dressings, including being strongly adhesive to tissues via covalent cross-linking, thermoresponsive shrinkage ability to contract the wounds mechanically, modulating inflammation, promoting neovascularization, and ease of storage and use. Such PNIPAm-P hydrogel could effectively accelerate the wound healing process in both a full-thickness skin defect mouse model and a partial-thickness skin defect porcine model via a synergistic effect, including being strongly adhesive to tissues, mechanically contracting the wounds, promoting angiogenesis, depositing collagen, and reducing inflammation. Moreover, such PNIPAm-P hydrogel also exhibits a wide range of applications in other biomedical aspects, such as diabetic wound healing and tissue defect repair. Thus, such an easy-to-prepare and easily stored hydrogel dressing may provide new opportunities for wound healing, and point a new direction in the fields of bio-stents and drug delivery, together with wearable or implantable medical devices.

EXPERIMENTAL PROCEDURES

Resource availability

Lead contact

Further information and requests for resources and reagents should be directed to and will be fulfilled by the lead contact, Qian Chen (chenqian@suda.edu.cn).

Materials availability

The materials generated in this study are available from the corresponding author upon request.

Data and code availability

The data used to support the findings of this study are available from the corresponding author upon request.

Materials, cell lines, and animals

MAA was purchased from Damas-beta. Gelatin, N,N'-methylene bisacrylamide (MBAA), and STZ were purchased from Macklin. NIPAm and N,N,N',N'-tetramethyl-ethylenediamine (TEMED) were purchased from J&K Scientific Co. Acrylamide (AAm) and ammonium persulphate (APS) were purchased from Energy Chemical. Anti-mouse CD11b antibody-PE, anti-mouse F4/80 antibody-PerCP, and anti-mouse CD206 antibody-APC were purchased from BioLegend. All solvents and chemicals were purchased from commercial sources and used as received, unless otherwise noted. NIH-3T3 fibroblast cells were cultured in Dulbecco's modified

Eagle medium (DMEM) (HyClone, United States) containing 1% penicillin-streptomycin and 10% fetal bovine serum (HyClone, United States) under standard conditions (37°C and 5% CO₂). BALB/c mice and C57BL/6 mice (6–8 weeks) were purchased from Changzhou Cavins Laboratory Animal Co (specific pathogen free). New Zealand white rabbits (3–5 months old) were purchased from Suzhou High-tech Zone Zhenhu Laboratory Animal Technology Co. Bama minipigs (3–4 months old) were purchased from Shanghai Jiaqian Biological Technology Co. All animal experiments were performed in compliance with the relevant laws and approved by the Institutional Animal Care and Use Committee of Soochow University (no. ECSU-2019000198).

Preparation of PNIPAm-P hydrogels

To prepare PNIPAm-P hydrogel, PMAA (6 kDa from gel permeation chromatography [GPC]) was first synthesized via traditional free radical polymerization and incubated with sodium hydroxide overnight to obtain PMAA in the form of sodium (PMAA-Na). First, an aqueous solution of NIPAm at the concentration of 100 mg/mL was prepared by dissolving the weighed amount of NIPAm in water (solution A). Second, an aqueous solution of gelatin at the concentration of 25 mg/mL was prepared by dissolving the weighed amount of gelatin in water (solution B). Third, solution B, PMAA-Na (25 mg/mL), and cross-linking agent MBAA, were slowly added to solution A (solution C). After uniformly mixing, solution C was bubbled under N₂ for 30 min to remove oxygen. Finally, initiator APS and accelerator TEMED were added into solution C and reacted at 4°C for 6–8 h to obtain PNIPAm-P hydrogel. After gelation, the hydrogel was taken out and cut into small pieces, soaked in phosphate buffer saline (PBS) for 30 min, and rinsed three times before use. This hydrogel could be lyophilized for storage.

Characterization

The morphological structures of these hydrogels at 25°C and 37°C were observed using a scanning electron microscope (ZEISS G500, Germany). The thermal response behavior of hydrogel was evaluated by placing the hydrogel at 37°C and measuring the volume change over time. The initial size and final size were denoted as l₀ and l, and the area strain was calculated by $1 - (l_0/l)^2$.

Wound healing *in vivo*

In order to verify the effectiveness of PNIPAm-P hydrogel for wound healing, we placed it on the skin wounds of rodents. First, the backs of mice were shaved and disinfected with iodophor and 75% alcohol, and then two wounds were established on the backs of mice (one on each side) using a dermatome (diameter: 6 mm). Three groups of different hydrogel dressings, including PAAm-P, PNIPAm, and PNIPAm-P, were applied to the wounds. Then, additional materials and medical bandages were used to cover the wound area to minimize water loss and prevent animal scratches.

In addition to the mouse wound model, a porcine partial-thickness wound model, which is similar to human, was used here. In this experiment, the backs of minipigs were shaved and disinfected with iodophor and 75% alcohol, and then eight partial-thickness (750 μm deep, 2.5 × 2.5 cm) wounds (four on each side) were established using a dermatome. The minimum distance between wounds was kept at 4 cm. Then, the PNIPAm-P hydrogel dressings were applied to the wounds on the right, and the wounds on the left were used as the control. Then, the wounds were covered with a layer of transparent dressing and secured with skin staples. For further protection, a layer of soft self-adhesive bandage was used to support and protect the underlying dressing. After the experiment, the minipigs were

monitored for any discomfort, their dressings were removed, and the wounds were imaged and recorded by sterile ruler measurement every 2 days.

Moreover, a diabetic wound model on mice was established. Specially, a diabetic mouse model was induced by intraperitoneal injection of STZ (50 mg/kg) for 5 days. Mice whose fasting blood glucose levels were higher than 11.1 mmol/L were used in this experiment. The wound model and therapeutic process were carried out according to the above-mentioned method. The wounds were observed and recorded every 2 days, with measurements and analysis by ImageJ software.

Wound tissue microenvironment assessment

In the mouse wound model, the mice were sacrificed and their wound tissues were collected to investigate the changes in the wound microenvironment on day 5 after different treatments. In detail, the surrounding wound tissues of different groups were first collected and then fixed with 4% paraformaldehyde for histological evaluation by H&E staining. As shown in [Figure S5A](#), the regenerated tissue in wounds treated by PNIPAm-P hydrogel was thicker than that in the other three groups. The quality of newly regenerated tissues was further confirmed by the magnified micrographs, as shown in [Figure S5B](#). Many new blood vessels existed in the regenerated area of samples treated with PNIPAm-P hydrogel. In a parallel experiment, the freshly collected wound tissues were digested with collagenase (1 mg/mL) and hyaluronidase (1 mg/mL) at 37°C, stained with corresponding fluorescently labeled antibodies, and analyzed by flow cytometry. The gating strategy and FMO (fluorescence minus one) control of macrophages, M1-like macrophages, and M2-like macrophages are given in [Figures S7](#) and [S8](#). In the meantime, for immunofluorescence staining, the freshly collected wound tissues were also fixed with optimal cutting temperature compound and cut into slices with the cryostat (Leica, Germany), and then stained with corresponding antibodies according to standard method. The immunofluorescence staining slides were observed by a confocal microscope (ZEISS, Germany) followed by quantifying using ImageJ. Moreover, the concentrations of different cytokines, including IL-1 β , IL-6, IL-10, and TNF- α , around the wounds were measured with ELISA kits according to the manufacturer's instructions (Thermo Fisher, cat. no. 88-7013-88, cat. no. 88-7064-88, cat. no. 88-7105-88, cat. no. 88-7324-88). Then, the formation of functional blood vessels was assessed using the Oxy-Hemo mode in the Vevo LAZR system (Verasonics Inc., Canada), and the average blood oxygen saturation (sO_2) level in the new tissues was quantified using the Vevo software. For the porcine partial-thickness wound model, the surrounding wound tissues were collected and fixed with 4% paraformaldehyde for H&E, Masson trichrome, and PSR staining. The levels of IL-1 β , IL-6, IL-10, and TNF- α around the wounds were measured with ELISA kits (Thermo Fisher, cat. no. ESIL1B, cat. no. ESIL6, cat. no. KSC0101, cat. no. ES24RB).

Potential repair effects on ex vivo organs

In order to evaluate the contraction effect of PNIPAm-P hydrogel on ex vivo organs, the rabbits were sacrificed and their major organs, including heart, kidney, stomach, and liver, were collected. The tissue defect (8 mm) on each organ was created using a hole punch and covered with PNIPAm-P hydrogel. Then, these organs were placed in an environment with the temperature at 37°C. Two hours later, the hydrogel was peeled off and the wound area was recorded and calculated by ImageJ software.

Statistical analysis

All statistical analyses were evaluated by GraphPad Prism (7.0). All data were presented as the mean \pm standard error of the mean (SEM). Two-tailed Student's t

test was used for two-group comparison and one-way analysis of variance (ANOVA) with a Tukey post hoc test was used for multiple comparisons. The threshold for statistical significance was * $p < 0.05$, ** $p < 0.01$, *** $p < 0.001$, **** $p < 0.0001$.

SUPPLEMENTAL INFORMATION

Supplemental information can be found online at <https://doi.org/10.1016/j.matt.2021.06.044>.

ACKNOWLEDGMENTS

This article was partially supported by the National Research Programs of China (2016YFA0201200, 2020YFA0211100), the National Natural Science Foundation of China (91959104, 21927803, 51903182, 51525203), the China Postdoctoral Science Foundation (2019M661936), the Natural Science Foundation of Jiangsu Province (BK20190826), Collaborative Innovation Center of Suzhou Nano Science and Technology, and the 111 Program from the Ministry of Education of China.

AUTHOR CONTRIBUTIONS

Q.C. and Z.L. oversaw all research. J.H., T.W., and Y.H. performed preparation and characterization of hydrogel. J.H., T.W., H.Z., M.C., and J.S. performed immune experiments. J.H., W.T., H.Z., M.C., Q.J., Y.T., H.Z., N.Y., L.C., and Z.X. performed cell and animal experiments. Q.C., J.H., and T.W. wrote the manuscript.

DECLARATION OF INTERESTS

A patent describing the hydrogel dressing for wound healing in this article was filed with the China Patent Bureau on March 10, 2021. Q.C., Z.L., and J.H. are inventors of the patent no. 2021102606213 application, which has not yet been made public. The authors declare no competing interests.

Received: January 25, 2021

Revised: May 31, 2021

Accepted: June 25, 2021

Published: July 28, 2021

REFERENCES

1. Sen, C.K., Gordillo, G.M., Roy, S., Kirsner, R., Lambert, L., Hunt, T.K., Gottrup, F., Gurtner, G.C., and Longaker, M.T. (2009). Human skin wounds: a major and snowballing threat to public health and the economy. *Wound Repair Regen.* 17, 763–771.
2. Puthia, M., Butrym, M., Petrlova, J., Strömdahl, A.-C., Andersson, M.Å., Kjellström, S., and Schmidtchen, A. (2020). A dual-action peptide-containing hydrogel targets wound infection and inflammation. *Sci. Transl. Med.* 12, eaax6601.
3. Sun, B.K., Siprashvili, Z., and Khavari, P.A. (2014). Advances in skin grafting and treatment of cutaneous wounds. *Science* 346, 941–945.
4. Boothby, I.C., Cohen, J.N., and Rosenblum, M.D. (2020). Regulatory T cells in skin injury: at the crossroads of tolerance and tissue repair. *Sci. Immunol.* 5, eaaz9631.
5. Martin, P., and Leibovich, S.J. (2005). Inflammatory cells during wound repair: the good, the bad and the ugly. *Trends Cell Biol.* 15, 599–607.
6. Zhang, Z., Chen, Z., Wang, Y., and Zhao, Y. (2020). Bioinspired conductive cellulose liquid-crystal hydrogels as multifunctional electrical skins. *Proc. Natl. Acad. Sci. U S A* 117, 18310–18316.
7. Dyson, M., Young, S., Pendle, C.L., Webster, D.F., and Lang, S.M. (1988). Comparison of the effects of moist and dry conditions on dermal repair. *J. Invest. Dermatol.* 91, 434–439.
8. Yannas, I., Burke, J., Orgill, D., and Skrabut, E. (1982). Wound tissue can utilize a polymeric template to synthesize a functional extension of skin. *Science* 215, 174–176.
9. Li, X., He, Y., Hou, J., Yang, G., and Zhou, S. (2020). A time-programmed release of dual drugs from an implantable trilayer structured fiber device for synergistic treatment of breast cancer. *Small* 16, 1902262.
10. Yao, X., Zhu, G., Zhu, P., Ma, J., Chen, W., Liu, Z., and Kong, T. (2020). Omnipobic ZIF-8@Hydrogel membrane by microfluidic-emulsion-templating method for wound healing. *Adv. Funct. Mater.* 30, 1909389.
11. Shang, Y., Wang, Z., Zhang, R., Li, X., Zhang, S., Gao, J., Li, X., and Yang, Z. (2019). A novel thermogel system of self-assembling peptides manipulated by enzymatic dephosphorylation. *Chem. Commun.* 55, 5123–5126.
12. Guo, J., Sun, W., Kim, J.P., Lu, X., Li, Q., Lin, M., Mrowczynski, O., Rizk, E.B., Cheng, J., Qian, G., et al. (2018). Development of tannin-inspired antimicrobial bioadhesives. *Acta Biomater.* 72, 35–44.
13. Li, J., and Mooney, D.J. (2016). Designing hydrogels for controlled drug delivery. *Nat. Rev. Mater.* 1, 16071.
14. Mirani, B., Pagan, E., Currie, B., Siddiqui, M.A., Hosseinzadeh, R., Mostafalu, P., Zhang, Y.S., Ghahary, A., and Akbari, M. (2017). An advanced multifunctional hydrogel-based dressing for wound monitoring and drug delivery. *Adv. Healthc. Mater.* 6, 1700718.
15. Boateng, J.S., Matthews, K.H., Stevens, H.N.E., and Eccleston, G.M. (2008). Wound healing dressings and drug delivery systems: a review. *J. Pharm. Sci.* 97, 2892–2923.

16. Lin, S., Yuk, H., Zhang, T., Parada, G.A., Koo, H., Yu, C., and Zhao, X. (2016). Stretchable hydrogel electronics and devices. *Adv. Mater.* 28, 4497–4505.
17. Ci, T., Shen, Y., Cui, S., Liu, R., Yu, L., and Ding, J. (2017). Achieving high drug loading and sustained release of hydrophobic drugs in hydrogels through *in situ* crystallization. *Macromol. Biosci.* 17, 1600299.
18. Brown, B.N., Londono, R., Tottey, S., Zhang, L., Kukla, K.A., Wolf, M.T., Daly, K.A., Reing, J.E., and Badylak, S.F. (2012). Macrophage phenotype as a predictor of constructive remodeling following the implantation of biologically derived surgical mesh materials. *Acta Biomater.* 8, 978–987.
19. Talior-Volodarsky, I., Mahou, R., Zhang, D., and Sefton, M. (2017). The role of insulin growth factor-1 on the vascular regenerative effect of MAA coated disks and macrophage-endothelial cell crosstalk. *Biomaterials* 144, 199–210.
20. Lisovsky, A., Zhang, D.K.Y., and Sefton, M.V. (2016). Effect of methacrylic acid beads on the sonic hedgehog signaling pathway and macrophage polarization in a subcutaneous injection mouse model. *Biomaterials* 98, 203–214.
21. Carleton, M.M., and Sefton, M.V. (2019). Injectable and degradable methacrylic acid hydrogel alters macrophage response in skeletal muscle. *Biomaterials* 223, 119477.
22. Fan, Z., Deng, J., Li, P.Y., Chery, D.R., Su, Y., Zhu, P., Kambayashi, T., Blankenhorn, E.P., Han, L., and Cheng, H. (2019). A new class of biological materials: cell membrane-derived hydrogel scaffolds. *Biomaterials* 197, 244–254.
23. Lisovsky, A., and Sefton, M.V. (2016). Shh pathway in wounds in non-diabetic Shh-Cre-eGFP/Ptch1-LacZ mice treated with MAA beads. *Biomaterials* 102, 198–208.
24. Fitzpatrick, L.E., Lisovsky, A., and Sefton, M.V. (2012). The expression of sonic hedgehog in diabetic wounds following treatment with poly(methacrylic acid-co-methyl methacrylate) beads. *Biomaterials* 33, 5297–5307.
25. Mahou, R., Zhang, D.K.Y., Vlahos, A.E., and Sefton, M.V. (2017). Injectable and inherently vascularizing semi-interpenetrating polymer network for delivering cells to the subcutaneous space. *Biomaterials* 131, 27–35.
26. Blacklow, S.O., Li, J., Freedman, B.R., Zeidi, M., Chen, C., and Mooney, D.J. (2019). Bioinspired mechanically active adhesive dressings to accelerate wound closure. *Sci. Adv.* 5, eaaw3963.
27. Wang, Y., Shang, L., Chen, G., Sun, L., Zhang, X., and Zhao, Y. (2020). Bioinspired structural color patch with anisotropic surface adhesion. *Sci. Adv.* 6, eaax8258.
28. Martin, P., and Lewis, J. (1992). Actin cables and epidermal movement in embryonic wound healing. *Nature* 360, 179–183.
29. Nodder, S., and Martin, P. (1997). Wound healing in embryos: a review. *Anat. Embryol. (Berl.)* 195, 215–228.
30. Zhu, M., Zhang, F., and Chen, X. (2020). Bioinspired mechanically interlocking structures. *Small Struct.* 1, 2000045.
31. Yuk, H., Varela, C.E., Nabzdyk, C.S., Mao, X., Padra, R.F., Roche, E.T., and Zhao, X. (2019). Dry double-sided tape for adhesion of wet tissues and devices. *Nature* 575, 169–174.
32. Shi, Y., Ma, C., Peng, L., and Yu, G. (2015). Conductive “smart” hybrid hydrogels with PNIPAM and nanostructured conductive polymers. *Adv. Funct. Mater.* 25, 1219–1225.
33. Qiu, Y., and Park, K. (2001). Environment-sensitive hydrogels for drug delivery. *Adv. Drug Deliv. Rev.* 53, 321–339.
34. Cai, S., and Suo, Z. (2011). Mechanics and chemical thermodynamics of phase transition in temperature-sensitive hydrogels. *J. Mech. Phys. Solids* 59, 2259–2278.
35. Hirokawa, Y., and Tanaka, T. (1984). Volume phase transition in a non-ionic gel. *AIP Conf. Proc.* 107, 203–208.
36. Chen, Y., Shi, J., Zhang, Y., Miao, J., Zhao, Z., Jin, X., Liu, L., Yu, L., Shen, C., and Ding, J. (2020). An injectable thermosensitive hydrogel loaded with an ancient natural drug colchicine for myocardial repair after infarction. *J. Mater. Chem. B* 8, 980–992.
37. Wynn, T.A., and Vannella, K.M. (2016). Macrophages in tissue repair, regeneration, and fibrosis. *Immunity* 44, 450–462.
38. Lee, J.-H., Parthiban, P., Jin, G.-Z., Knowles, J.C., and Kim, H.-W. (2020). Materials roles for promoting angiogenesis in tissue regeneration. *Prog. Mater. Sci.* 117, 100732.
39. Feng, Z., Su, Q., Zhang, C., Huang, P., Song, H., Dong, A., et al. (2020). Bioinspired nanofibrous glycopeptide hydrogel dressing for accelerating wound healing: a cytokine-free, M2-type macrophage polarization approach. *Adv. Funct. Mater.* 30, 2006454.
40. Xi-Qiao, W., Ying-Kai, L., Chun, Q., and Shu-Liang, L. (2009). Hyperactivity of fibroblasts and functional regression of endothelial cells contribute to microvessel occlusion in hypertrophic scarring. *Microvasc. Res.* 77, 204–211.
41. Stojadinovic, A., Elster, E.A., Anam, K., Tadaki, D., Amare, M., Zins, S., and Davis, T.A. (2008). Angiogenic response to extracorporeal shock wave treatment in murine skin isografts. *Angiogenesis* 11, 369–380.
42. Zhao, H., Huang, J., Li, Y., Lv, X., Zhou, H., Wang, H., Xu, Y., Wang, C., Wang, J., and Liu, Z. (2020). ROS-scavenging hydrogel to promote healing of bacteria infected diabetic wounds. *Biomaterials* 258, 120286.
43. Zhu, Y., Zhang, J., Song, J., Yang, J., Du, Z., Zhao, W., Guo, H., Wen, C., Li, Q., Sui, X., et al. (2020). A multifunctional pro-healing zwitterionic hydrogel for simultaneous optical monitoring of pH and glucose in diabetic wound treatment. *Adv. Funct. Mater.* 30, 1905493.
44. Wang, S., Zheng, H., Zhou, L., Cheng, F., Liu, Z., Zhang, H., Wang, L., and Zhang, Q. (2020). Nanoenzyme-reinforced injectable hydrogel for healing diabetic wounds infected with multidrug resistant bacteria. *Nano Lett.* 20, 5149–5158.
45. Falanga, V. (2005). Wound healing and its impairment in the diabetic foot. *Lancet* 366, 1736–1743.
46. Hu, X., Zhang, H., Wang, Z., Shiu, C.Y.A., and Gu, Z. (2021). Microneedle array patches integrated with nanoparticles for therapy and diagnosis. *Small Struct.* 2, 2000097.
47. Yu, J., Wang, J., Zhang, Y., Chen, G., Mao, W., Ye, Y., Kahkoska, A.R., Buse, J.B., Langer, R., and Gu, Z. (2020). Glucose-responsive insulin patch for the regulation of blood glucose in mice and minipigs. *Nat. Biomed. Eng.* 4, 499–506.
48. Wang, J., Ye, Y., Yu, J., Kahkoska, A.R., Zhang, X., Wang, C., Sun, W., Corder, R.D., Chen, Z., Khan, S.A., et al. (2018). Core-shell microneedle gel for self-regulated insulin delivery. *ACS Nano* 12, 2466–2473.